YALE
PEABODY
MUSEUM

P.O. BOX 208118 | NEW HAVEN CT 06520-8118 USA | PEABODY.YALE. EDU

JOURNAL OF MARINE RESEARCH

The *Journal of Marine Research,* one of the oldest journals in American marine science, published important peer-reviewed original research on a broad array of topics in physical, biological, and chemical oceanography vital to the academic oceanographic community in the long and rich tradition of the Sears Foundation for Marine Research at Yale University.

An archive of all issues from 1937 to 2021 (Volume 1–79) are available through EliScholar, a digital platform for scholarly publishing provided by Yale University Library at https://elischolar.library.yale.edu/.

Requests for permission to clear rights for use of this content should be directed to the authors, their estates, or other representatives. The *Journal of Marine Research* has no contact information beyond the affiliations listed in the published articles. We ask that you provide attribution to the *Journal of Marine Research*.

Yale University provides access to these materials for educational and research purposes only. Copyright or other proprietary rights to content contained in this document may be held by individuals or entities other than, or in addition to, Yale University. You are solely responsible for determining the ownership of the copyright, and for obtaining permission for your intended use. Yale University makes no warranty that your distribution, reproduction, or other use of these materials will not infringe the rights of third parties.

This work is licensed under a Creative Commons Attribution-NonCommercial-ShareAlike 4.0 International License.
https://creativecommons.org/licenses/by-nc-sa/4.0/

The New Zealand semi-diurnal tide

by J. A. T. Bye[1] and R. A. Heath[2]

ABSTRACT

Data on the semi-diurnal tide around the coast of New Zealand, and on neighbouring islands are summarized, and interpreted using World, and a large scale, numerical models, and an analytical island-shelf model. The island-shelf model consists of a circular island (representing New Zealand) surrounded by a parabolic shelf, and a deep ocean of constant depth.

The basic feature of the semi-diurnal tide is a complete range of phase (0°–360°) around the New Zealand coast, with large changes in the age of the tide from region to region, and an approximate threefold amplification in tidal amplitude over the deep sea at the coast. All these features are explained through weak trapping of the semi-diurnal tidal constituents on the New Zealand shelf, together with a changing direction of propagation towards New Zealand of the constituents, which varies from approximately north-west for the M_2 tide to north-east for the S_2 tide.

1. Introduction

Very little has been published on the New Zealand tides to date, apart from that appearing as information mainly for mariners in the New Zealand Pilots (e.g. Hydrographic Department 1958), the Admiralty Tide Table (e.g. Hydrographic Department, Admiralty 1963), and on the Navy Department Hydrographic Charts.

The New Zealand tidal regime is unique in that the phase of the major components, the principal lunar and solar semi-diurnal constituents (M_2, S_2) embrace the complete range from 0 to 360 degrees. Although the phase distribution is similar to that around an amphidrome, the coastal tidal amplitudes are large (Nelson and Onehunga [Fig. 1, Table 1] have the largest recorded M_2 amplitudes of 1.31 m) compared with amplitudes on neighbouring islands.

The ratio of the amplitude of the two main semi-diurnal tides M_2 and S_2 falls into four main geographical groups (Fig. 2, Table 1); [A] a group on the west coast with a ratio around 0.25; [B] a group on the north-east coast with a ratio around 0.15; [C] a group on the east coast north of the Chatham Rise (Fig. 1) with a ratio near 0.05; [D] a group on the east coast south of the Chatham Rise with a ratio near 0.13. The two areas that do not fit simply into this grouping are the Cook Strait region

1. The Flinders Institute for Atmospheric and Marine Sciences, Flinders University of South Australia, Bedford Park, South Australia, 5042.

2. New Zealand Oceanographic Institute, Department of Scientific and Industrial Research, Wellington, New Zealand.

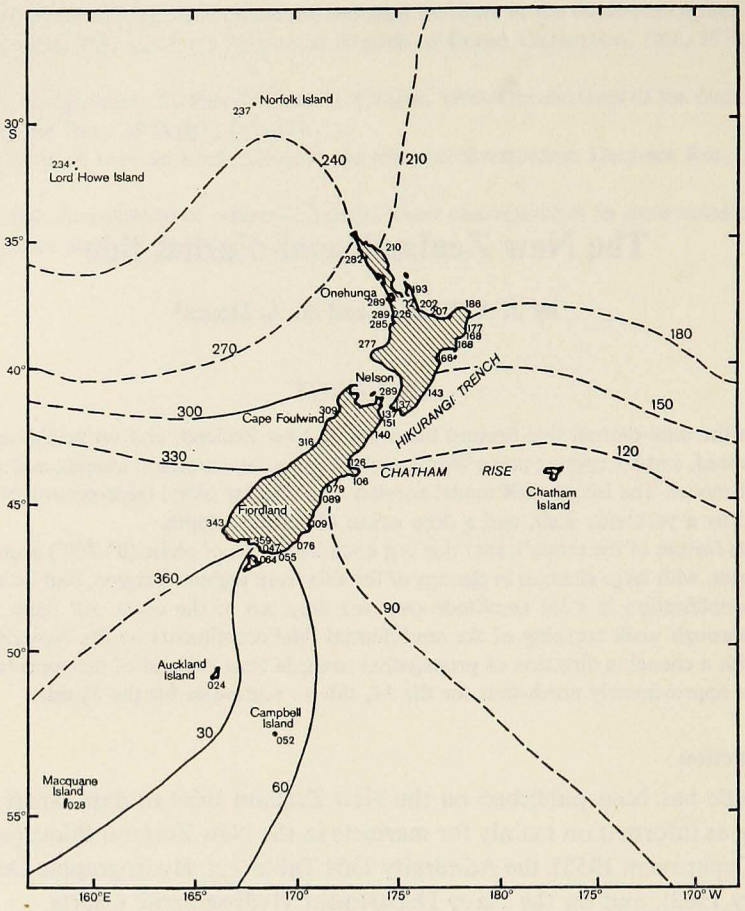

Figure 1. Contours of the observed phase of the principal lunar semi-diurnal tidal constituent (M_2). The observed values of the phase are also shown.

and the islands south of New Zealand. However, the M_2 tides in Cook Strait are small, a consequence of the 120° phase change in this component through the Strait (Heath, in press), and the relative amplitudes on the southern islands are probably determined by the influence of the extensive bathymetric platform of the Campbell Plateau.

The limited current measurements made on the New Zealand continental shelf indicate that, in general, the tidal current speeds are of the order of 5–10 times greater than the mean current (Carter and Heath, in press, Fig. 3).

The explanation for the phase distribution of the New Zealand semi-diurnal tide may be that it indicates the presence of a semi-diurnal trapped wave. This possibility is evident from the fact that the resonant period of a wave travelling on a smoothed 2000 m isobath around New Zealand at the shallow water wave speed, is about

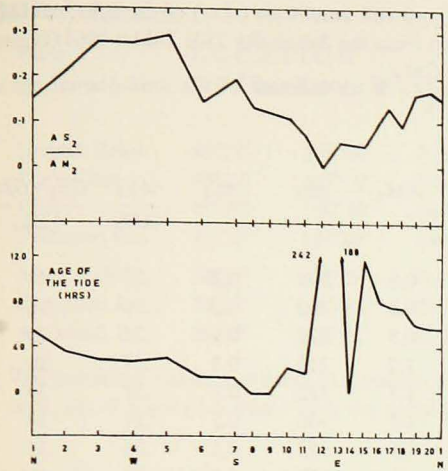

(a)

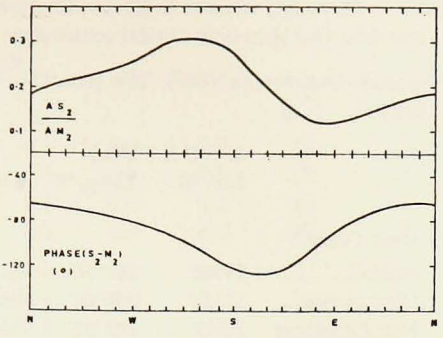

(b)

Figure 2. The variation of the ratio of the amplitudes of the M_2 and S_2 tidal constituents, and the age of the tide around New Zealand.

(a) Observed.

KEY TO FIGURE: The numbers refer to places round the New Zealand coast given in Table 1. The Cardinal points indicate their approximate orientation.

1	Russell	6	Deep Cove	11	Lyttelton	16	Gisborne
2	Raglan	7	Bluff	12	Kaikoura	17	Hicks Bay
3	New Plymouth	8	Port Chalmers	13	Wellington	18	Tauranga
4	Westport	9	Timaru	14	Castlepoint	19	Auckland
5	Greymouth	10	Akaroa	15	Napier	20	Whangarei

(b) From solutions of the island-shelf model (the age of the tide = Phase of $(S_2 - M_2)$ (°)/1.016).

13 hrs. The relatively large differences in the ratio of the M_2 to the S_2 tide from region to region suggests however, that the phenomenon is not simple.

In this paper we explore the trapping hypothesis in detail. First, use is made of the age of the tides as a measure of resonance around New Zealand. Second, because very little offshore tidal data is available for comparison with a trapped wave solution, and because the grid size of the existing world tidal models is too large. A large scale numerical model is used to describe the tides in more detail.

Finally, an analytical solution for a parabolic shelf (representing the New Zealand continental shelf) surrounded by a region of constant depth (representing the deep ocean) is developed.

2. The age of the tide as a measure of resonance

The age of the tide is the time interval between the time of new or full moon, when the equilibrium semi-diurnal tide is at a maximum, and the time of local

Table 1. Phase (g^0, referred to Greenwich Mean Time) and amplitude ($A\,m$) of the principal (M_2) and solar (S_2) semi-diurnal tidal constituents taken from the Admiralty Tide Tables 1964 (Hydrographic Department 1963). The quantity $\frac{GS_2 - GM_2}{1.016}$ is an estimate of the semi-diurnal age of the tide.

Place	LOCATION Lat. °S	Long. °E	gM_2	AM_2	gS_2	AS_2	$\frac{AS_2}{AM_2}$	$\frac{GS_2-GM_2}{1.016}$
A *West Coast*								
Norfolk.....	29°04′	167°56′	237	0.6	294	0.2	.26	44
Lord Howe...	31°32′	159°04′	234	0.6	260	0.2	.26	14
New Caledonia	22°02′	166°08′	235	0.5	273	0.1	.27	25
New Plymouth	39°04′	174°03′	277	1.2	318	0.3	.275	28
Kawhia.....	38°04′	174°49′	285	1.1	332	0.3	.27	34
Raglan.....	37°48′	174°53′	289	1.1	336	0.2	.21	34
Manukau.....	37°03′	174°31′	289	1.1	333	0.3	.26	31
Onehunga	36°56′	174°47′	304	1.3	358	0.3	.26	41
Hokianga.....	35°24′	173°31′	289	1.1	340	0.3	.24	38
Westport.....	41°44′	171°36′	309	1.1	349	0.3	.27	27
Greymouth...	42°26′	171°13′	316	0.9	359	0.3	.29	30
Cook Strait *Tasman Bay*								
Makara.....	41°13′	174°37′	255	0.3	346	0.2	.7	78
Porirua.....	41°06′	174°52′	289	0.4	355	0.2	.54	53
Nelson.....	41°16′	173°16′	280	1.3	335	0.4	.30	42
Greville.....	40°52′	173°48′	272	1.2	324	0.5	.39	39
B *North-East Coast*								
Russell.....	35°16′	174°07′	210	0.8	279	0.1	.15	56
Whangarei....	35°49′	174°30′	213	0.9	283	0.2	.17	57
Auckland.....	36°51′	174°46′	204	1.1	278	0.2	.16	61
Great Barrier .	36°09′	175°19′	199	0.9	284	0.1	.14	72
Tauranga.....	37°39′	176°11′	202	0.7	290	0.1	.09	75
Hicks Bay....	37°34′	178°19′	186	0.7	275	0.1	.13	76
C *East Coast*	(North of Chatham Rise)							
Gisborne.....	38°41′	178°02′	168	0.6	262	0.1	.1	81
Napier.....	39°29′	176°55′	166	0.6	297	0.0	.05	117
Castlepoint ...	40°55′	176°13′	143	0.6	153	0.0	.05	−2
Wellington....	41°17′	174°47′	137	0.5	340	0.0	.06	188
Cape Campbell	41°44′	174°15′	151	0.6	288	0.0	.05	123
Kaikoura.....	42°24′	173°42′	140	1.0	038	0.0	.00	242
D *East Coast*	(South of Chatham Rise)							
Lyttelton.....	43°36′	172°44′	126	0.9	155	0.1	.07	17
Akaroa.....	43°48′	172°55′	106	0.9	141	0.1	.11	22
Timaru.....	44°24′	171°15′	079	0.8	089	0.1	.13	−2
Port Chalmers	45°49′	170°38′	109	0.7	120	0.1	.13	−1

Table 1 (continued).

Place	LOCATION							
	Lat. °S	Long. °E	gM_2	AM_2	gS_2	AS_2	$\frac{AS_2}{AM_2}$	$\frac{GS_2 - GM_2}{1.016}$
Nugget Point .	46°27′	169°49′	079	0.7	094	0.1	.13	6
Deep Cove ...	45°27′	167°10′	343	0.7	008	0.1	.13	13
Bluff.....	46°36′	168°20′	047	0.9	073	0.2	.17	14
Patterson In...	46°54′	168°07′	044	0.8	058	0.2	.19	2
Macquarie I ..	54°31′	158°58′	028	0.3	069	0.1	.3	28
Campbell I ...	52°33′	169°13′	052	0.4	064	0.1	.31	0
Auckland I ...	50°52′	166°05′	024	0.4	051	0.1	.33	15

* The published phases g relative to Greenwich Mean Time have been converted to local standard time, i.e. $G = g - 12\,\omega$ where ω is the corresponding angular frequency.

spring tide. Near the semi-diurnal frequency an estimate of the age of the tide is given by

$$\frac{\partial\theta}{\partial\omega} = \frac{\text{Phase of } (S_2 - M_2)}{\text{Speed of } (S_2 - M_2)} = \frac{\text{Phase of } (S_2 - M_2)}{1.016} \text{ hours.}$$

(Lamb, 1953, p. 224). The age of the tide for the New Zealand region (Table 1, Fig. 2) varies between about 5 hrs. and 75 hrs., except for the region near the Cook Strait where the S_2 tide has a very small amplitude. All around New Zealand there is also a weak maximum in the admittance near the M_2 frequency, and a progressive phase change across the semi-diurnal components (Fig. 3).

Arguments for proposing the age of the tide as a measure of resonance have been advanced by drawing an analogy with a simple harmonic oscillator (Garrett and Munk, 1971), and Webb (1973a) has concluded that regions in the ocean where the age of the tide is large, correspond to localized resonances. The significance of the New Zealand observations will be discussed in Section 4 after the analytical model for the tide has been considered.

3. Numerical models

There are several tidal charts produced from global models of the M_2 tide, which show co-range and co-tidal lines in the vicinity of New Zealand (Hendershott, 1973). All solutions except Pekeris and Accad (1969) show the complete range of co-tidal lines, progressing in an anticlockwise sense around New Zealand with an amplification adjacent to the sub-continent. The radial character of the co-tidal lines is evident out to some 1500 km. Beyond this range, there are amphidromic points to the east and south-east (clockwise) and to the north-east (anticlockwise), and a region of tidal resonance off north-east Australia (Webb, 1973b). The groupings of the amplitude ratios of the M_2 and S_2 tides appear to be associated with these features (Bogdanov and Magarik, 1967). There is, however, considerable variability from model to

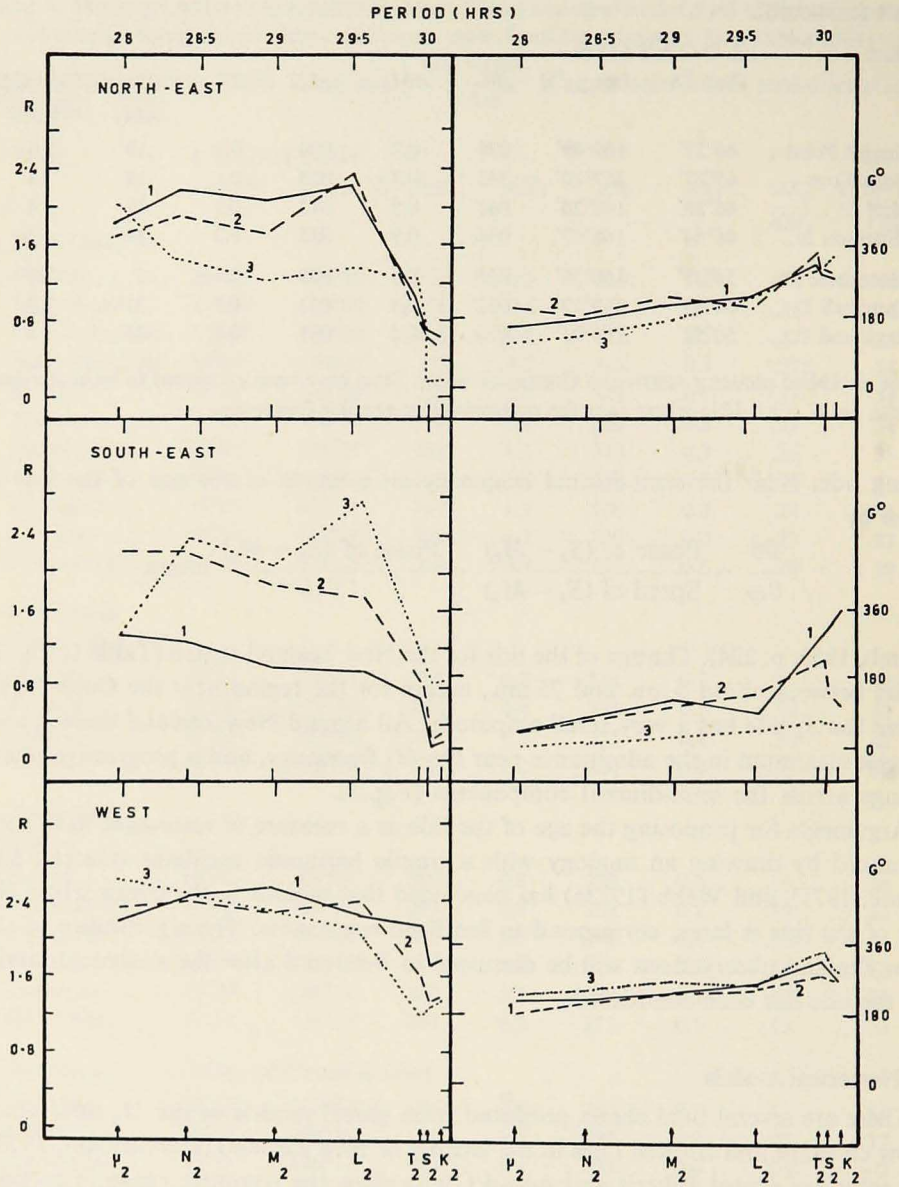

Figure 3. The phase (G^0) and the admittance (R) of the semi-diurnal tidal components μ_2, N_2, M_2, L_2, T_2, S_2, K_2. The admittance shown is the amplitude of the tidal constituent divided by the amplitude of the equilibrium tide (Doodson and Warburg 1941). Harmonic constants used are the mean for harmonic analysis of several individual years kindly made available by the New Zealand Lands and Surveys Department.

KEY TO FIGURE: The numbers refer to the following places on the New Zealand coast.

North-east.....	1	Auckland	2	Whangarei	3 Napier
South-east.....	1	Wellington	2	Lyttelton	3 Bluff
West	1	Nelson	2	Port Taranaki	3 Westport

model, and in no case is the resolution adequate to make a close study of the tidal amplification phenomenon. In this section, therefore, a rather more detailed examination is made, by enclosing New Zealand in a rectangle of dimensions 3000×3750 km. The boundary elevation, based on the data discussed previously, and the small scale numerical models, is taken to be a fundamental circular mode with the period of the M_2 tide, rotating about the centroid of the land area of the rectangle.

The numerical model is based on the equations: –

$$\frac{\partial U}{\partial t} - fV = -gH\frac{\partial \eta}{\partial x} - \frac{K}{H^2}(U^2 + V^2)^{1/2} U$$

$$\frac{\partial V}{\partial t} + fU = -gH\frac{\partial \eta}{\partial y} - \frac{K}{H^2}(U^2 + V^2)^{1/2} V$$

$$\frac{\partial \eta}{\partial t} + \frac{\partial U}{\partial x} + \frac{\partial V}{\partial y} = 0,$$

where H is the depth, η is the elevation of the sea surface above the undisturbed level, U and V are the volume transports along Ox (towards the east) and Oy (towards the north, $f = 2\Omega \sin \varphi$ is the Coriolis Parameter, where Ω is the angular velocity of the Earth, φ is latitude, g is the acceleration of gravity, and K is the coefficient of bottom friction. The numerical techniques are similar to those used by Matthews and Mungall (1972), and are fully described in Bye (1975).

The finite-difference network consisted of 27×33 lines, and the depths were obtained from Lawrence (1967). The finite-difference forcing on the boundary, corresponding approximately to a fundamental circular mode, is

$$\eta_{ij}(t) = ((i - i_0) A \sin \sigma t + (j - j_0) B \cos \sigma t) \Delta s$$

where (i, j) are the co-ordinates of the grid point on the boundary, (i_0, j_0) are the co-ordinates of the centroid of the model, Δs is the grid length, and σ is the angular frequency of the M_2 tide. The constants A and B were given the values 1.6×10^{-7} and -1.8×10^{-7} respectively, and the model was allowed to run for 10 complete tidal cycles, with $K = .0025$.

a. Results of the large-scale model. The results of the numerical model will be compared with those of the observed M_2 constituents alone, for, with only a limited shallow area defined by the mesh size, the observed small shallow water constituents (generated by the quadratic friction term) will not be well developed in the model.

(i) Comparison of Phases

The general pattern of the computed phases fits quite closely to those actually observed as might be expected for the analytical forcing was chosen to exhibit the overall 360° phase change on the outer boundary. However, the irregular phase

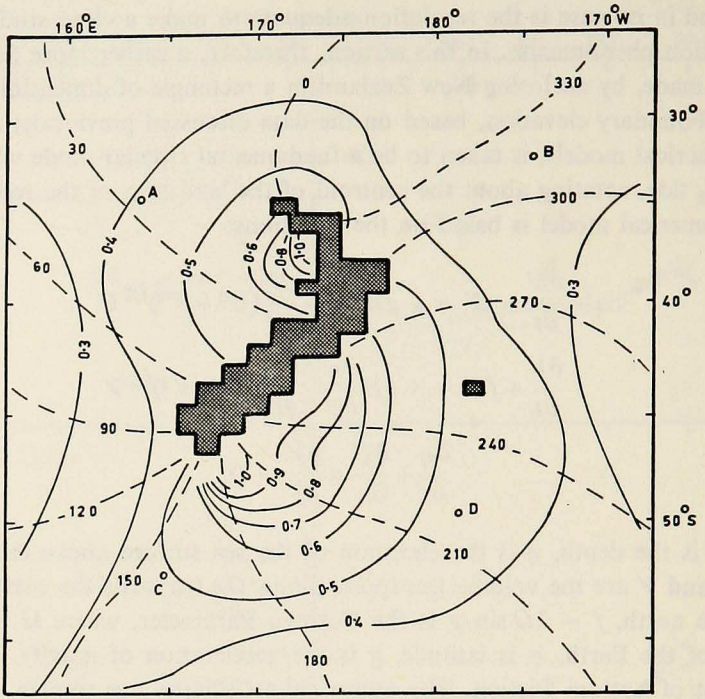

Figure 4. Contours of equal phase (°) and tidal amplitude (*m*) from the numerical model. Dashed lines are phase, solid lines are amplitude.

change with distance along the coast of New Zealand in the model, also agrees with that observed. In particular, the wave travels slowly over the shallow Campbell Plateau and Bounty Trough, around the southern end of New Zealand (Fig. 4), and up the east coast to the Chatham Rise. The wave then travels quickly up the Hikurangi Trench.

A list of the observed amplitudes and phases from islands or locations near deep water together with the values from the model are shown in Table 2. The model reproduces not only the general pattern but also the specific phases reasonably closely.

(ii) Comparison of Amplitude

The amplitudes on the southern and eastern part of the model are close to those observed, with the amplitude increasing strongly towards New Zealand, especially in the shallow areas. The amplitudes on the western side of the model are, however, somewhat smaller than observed values (Table 2).

(iii) Tidal Currents

Tidal ellipses of the tidal currents over the last cycle computed at four positions (A, B, C, D, in Fig. 4) one in each quadrant of the model are shown in Fig. 5. They

Table 2. Amplitude Am and phase g^0 of the observed M_2 tide, as deduced from the large scale numerical model. Difference in phase set to zero at Campbell Island.

	OBSERVED		MODEL	
Place	A	g	A	g
Campbell Island ...	0.4	052	0.5	052
Deep Cove.....	0.7	343	0.5	320
Nugget Point.....	0.73	079	0.8	095
Antipodes.....		100?	0.5	110
Chatham.....		100?		120
Kaikoura	1.06	140	1.1	140
Norfolk.....	0.58	237	0.4	200
Tauranga	0.7	202	0.5	200

are displayed solely to give an idea of the size of the flow in the model and should be regarded as very tentative.

The tidal current at these positions is at a maximum in the same direction as the wave phase velocity at high tide indicating that the wave is predominantly progressive. A complex structure of tidal currents was observed in the model with a tendency for flow parallel to the coast except over the shallow Chatham Rise, where strong on and off-shore currents are apparent. The total movement at any point is not more than a few kilometres. The direction of rotation of the tidal ellipses in the model agrees with that observed in the short term current measurements made by Heath (1973).

4. The analytical model

The approximate circular symmetry of the co-range lines and constant angular speed of the cotidal lines (Fig. 4), suggests a polar analytical representation of the semi-diurnal tide.

The polar equations of motion for an inviscid model are the following

$$\frac{\partial U}{\partial t} - fV = -gH\frac{\partial \eta}{\partial r} \tag{1}$$

$$\frac{\partial V}{\partial t} + fU = -\frac{gH}{r}\frac{\partial \eta}{\partial \theta} \tag{2}$$

where r is the radial co-ordinate

θ is the polar angle (increasing in a counterclockwise direction)

$U = uH$ in which u is the radial velocity

$V = vH$ in which v is the azimuthal velocity

and the continuity equation is

$$\frac{\partial \eta}{\partial t} + \frac{\partial U}{\partial r} + \frac{U}{r} + \frac{1}{r}\frac{\partial V}{\partial \theta} = 0.$$

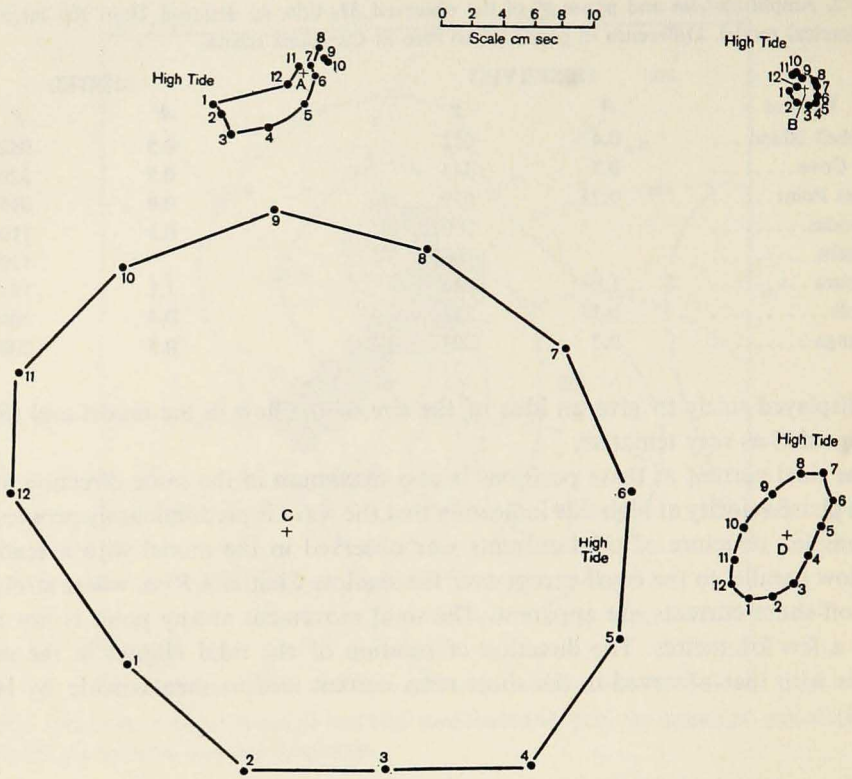

Figure 5. Tidal ellipses at four positions (A, B, C, D) shown in Figure 4.

The wave equation, derived by eliminating U and V; with the simplifying assumption of a constant Coriolis parameter has the form

$$\left[\nabla^2 - \frac{1}{gH}\left(\frac{\partial^2}{\partial t^2} + f^2\right) + \frac{1}{H}\left(\frac{1}{r^2}\frac{\partial H}{\partial \theta}\frac{\partial}{\partial \theta} + \frac{\partial H}{\partial r}\frac{\partial}{\partial r}\right)\right]\frac{\partial \eta}{\partial t} = \frac{f}{rH}\left(\frac{\partial H}{\partial \theta}\frac{\partial \eta}{\partial r} - \frac{\partial H}{\partial r}\frac{\partial \eta}{\partial \theta}\right) \tag{3}$$

where

$$\nabla^2 = \frac{\partial^2}{\partial r^2} + \frac{1}{r^2}\frac{\partial^2}{\partial \theta^2} + \frac{1}{r}\frac{\partial}{\partial r}.$$

The solution of equation (3) has been discussed extensively in the literature (e.g. Longuet-Higgins 1967, 1969; Summerfield 1969, 1972) in connection with the trapping of waves around islands. For two types of depth variation analytical solutions of equation (3) have been obtained. The two cases with their corresponding wave equations are;

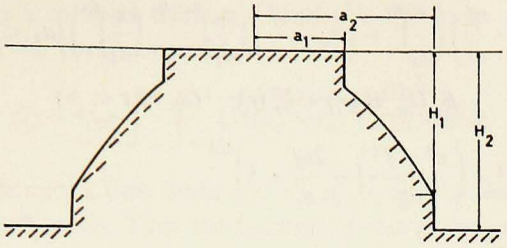

Figure 6. The island-shelf model.

(i) *Constant depth*

$$\left[\nabla^2 - \frac{1}{gH_2}\left(\frac{\partial^2}{\partial t^2} + f^2\right)\right]\eta = 0 \tag{4}$$

where H_2 is a constant depth.

(ii) *The parabolic shelf*

$$\left[r^2\frac{\partial^2}{\partial r^2} + 3r\frac{\partial}{\partial r} + \frac{\partial^2}{\partial \theta^2} - \frac{1}{\sigma_0^2}\left(\frac{\partial^2}{\partial t^2} + f^2\right)\right]\frac{\partial \eta}{\partial t} + 2f\frac{\partial \eta}{\partial \theta} = 0 \tag{5}$$

in which the constant σ_0 is the shelf parameter for the parabolic shelf given by

$$H = \sigma_0^2 r^2/g. \tag{6}$$

It is proposed to model the semi-diurnal tide around New Zealand by representing the bathymetry by a circular island surrounded by an inner parabolic shelf and an outer constant depth ocean basin (Fig. 6). The boundary conditions for the model (Longuet-Higgins, 1967) are,

$$\left.\begin{aligned} &U(r, \theta) = 0 \quad \text{at } r = a_1 \quad (a_1 > 0) \\ &\left.\begin{aligned}\eta(r, \theta)\\ U(r, \theta)\end{aligned}\right\} \text{ continuous at } r = a_2 \ (a_2 > a_1) \\ &\eta(r, \theta) = \zeta \quad \text{for } r \to \infty \end{aligned}\right\} \tag{7}$$

where a_1 is the radius of the circular island, a_2 is the radius at the edge of the parabolic shelf, and ζ is the far ocean elevation. The solution is obtained by a separation of variables as an infinite series of circular modes;

$$\eta = \sum_{n=-\infty}^{\infty} \eta_n^*(r) e^{i(n\theta - \sigma t)} \tag{8}$$

where n is the order of the mode of circular frequency σ ($\sigma > 0$). On substitution of equation (8) into equations (4) and (5) and applying the boundary conditions at $r = a_1$ and $r = \infty$, one obtains,

$$\eta_n^*(r) = \left\{ \begin{array}{c} A_n\left(\left(\varrho_4 - \frac{nf}{\sigma}\right)\left(\frac{r}{a_2}\right)^{\varrho_3} - \left(\sigma_3 - \frac{nf}{\sigma}\right)\left(\frac{a_1}{a_2}\right)^{\varrho_3-\varrho_4}\left(\frac{r}{a_2}\right)^{\varrho_4}\right)(a_1 \leqslant r < a_2) \\ B_n H_n^{(1)}(k_2 r) + \zeta_n^*(r) \quad (a_2 \leqslant r < \infty) \end{array} \right\} \tag{9}$$

where $\varrho_3 = -1 + \left(n^2 - \left(\frac{\sigma^2 - f^2}{\sigma_0^2}\right) + \frac{2nf}{\sigma} + 1\right)^{1/2}$,

$$\varrho_4 = -2 - \varrho_3,$$

$$k_2 = \left(\frac{1}{gH_2}(\sigma^2 - f^2)\right)^{1/2}, \quad \sigma > |f|,$$

and ζ_n^* is the n^{th} circular mode of a far ocean elevation,

$$\zeta = \sum_{n=-\infty}^{\infty} \zeta_n^*(r) e^{i(n\theta - \sigma t)}$$

which also satisfies equation (4).

The condition that $\sigma > |f|$ is satisfied by a semi-diurnal tidal constituent at all positions on Earth, except possibly very near the Poles, H_2 is the depth of the outer constant depth ocean basin, $H_n^{(1)}(x)$ is a Bessel function of the third kind (Hankel function), and A_n and B_n are arbitrary constants. The two equations which result from applying the boundary conditions at $r = a_2$ are,

$$\left(\left(\varrho_4 - \frac{nf}{\sigma}\right) - \left(\varrho_3 - \frac{nf}{\sigma}\right)\left(\frac{a_1}{a_2}\right)^{\varrho_3-\varrho_4}\right) A_n + (-H_n^{(1)}(k_2 a_2))B_n = \zeta_n^*(a_2) \tag{10}$$

$$\left.\begin{array}{c} \left(\varepsilon^2\left(\varrho_4 - \frac{nf}{\sigma}\right)\left(\varrho_3 - \frac{nf}{\sigma}\right)\left(1 - \left(\frac{a_1}{a_2}\right)^{\varrho_3-\varrho_4}\right)\right) A_n + \\ \left(-a_2 k_2 H_n^{(1)\prime}(k_2 a_2) + \frac{nf}{\sigma} H_n^{(1)}(k_2 a_2)\right) B_n = a_2 \zeta_n^{*\prime}(a_2) - \frac{nf}{\sigma}\zeta_n^*(a_2) \end{array}\right\} \tag{11}$$

where $\varepsilon = \left(\frac{H_1}{H_2}\right)^{1/2}$ in which H_1 is the depth of the parabolic shelf at $r = a_2$.

For the transient motion, the solution of equations (10) and (11) is an eigenvalue problem for σ (Summerfield, 1969), in which the A_n and B_n are determined by the initial conditions on η. The forced motion (which is pertinent to the tidal problem), however, is obtained by solving the equations for the A_n and B_n for a prescribed ζ.

The mode on the parabolic shelf is maintained by energy exchanges with the far ocean. It may be shown (Longuet-Higgins, 1967), that for the n^{th} circular mode the exchange flux (F_n) is given by,

$$F_n = \frac{2\varrho g\sigma}{k_2^2} B_n B_n^*$$

where the * denotes a complex conjugate, and ϱ is the water density. The energy (E_n) of the mode on the parabolic shelf is

$$E_n = {}^1/_2\varrho \int_{a_1}^{a_2}\int_0^{2\pi} \overline{(H(u_n^2 + v_n^2) + g\eta_n^2)}\, r\,d\theta\,dr$$

where the overbar denotes a time mean and η_n, u_n, v_n are the elevation, and velocity components of the n^{th} mode. Thus the fraction of energy lost per cycle is

$$\varphi_n = \frac{F_n T}{E_n}$$

φ_n, or more commonly $Q_n = 2\pi/\varphi_n$, is used as a measure of the degree of trapping of wave energy by the shelf; a high value of Q_n indicates a strongly trapped oscillation.

a. The parabolic shelf Kelvin wave. Before introducing the solutions in detail it is useful to consider the nature of the motion on the parabolic shelf. For the n^{th} circular mode, the radial velocity is,

$$u = iu_n^*(r)e^{i(n\theta - \sigma t)} \tag{12}$$

where

$$u_n^*(r) = \frac{g\sigma r^{-1}}{\sigma^2 - f^2}\left(\varrho_3 - \frac{nf}{\sigma}\right)\left(\varrho_4 - \frac{nf}{\sigma}\right)\left(\left(\frac{r}{a_2}\right)^{\varrho_3}\left(\frac{a_1}{a_2}\right)^{\varrho_3 - \varrho_4} - \left(\frac{r}{a_2}\right)^{\varrho_3}\right)\cdot A_n$$

$$\sigma \neq f$$

and the azimuthal velocity is

$$v = v_n^*(r)e^{i(n\theta - \sigma t)} \tag{13}$$

$$v_n^*(r) = \frac{gfr^{-1}}{\sigma^2 - f^2}\left(\left(\varrho_3 - \frac{nf}{\sigma}\right)\left(\varrho_4 - \frac{n\sigma}{f}\right)\left(\frac{r}{a_2}\right)^{\varrho_4}\left(\frac{a_1}{a_2}\right)^{\varrho_3 - \varrho_4} - \left(\varrho_3 - \frac{n\sigma}{f}\right)\left(\varrho_4 - \frac{nf}{\sigma}\right)\left(\frac{r}{a_2}\right)^{\varrho_3}\right)\cdot A_n$$

$$\sigma \neq f.$$

Thus, if either $\varrho_3 - \dfrac{nf}{\sigma} = 0$, or $\varrho_4 - \dfrac{nf}{\sigma} = 0$ the radial velocity is zero everywhere on the shelf. On substituting for ϱ_3 or ϱ_4 these conditions both reduce to the equation,

$$(\sigma^2 - f^2)(\sigma^2 - n^2\sigma_0^2) = 0. \tag{14}$$

The solution of equation (14) is

$$\sigma = n\sigma_0$$

and the properties of the corresponding circular mode are

$$\eta_n^* = \left(\frac{r}{a_2}\right)^{f/\sigma_0}\alpha \tag{15}$$

$$u_n^* = 0 \tag{16}$$

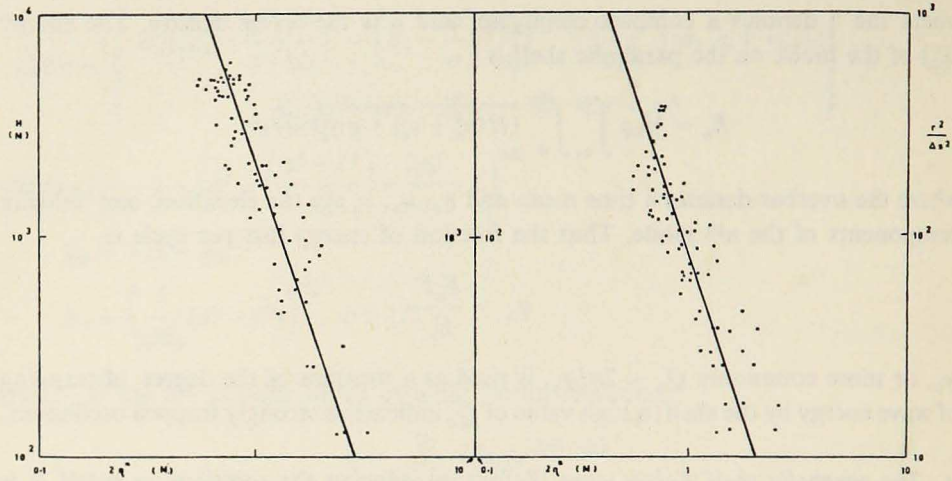

Figure 7(a). $1nH$ versus $1n2\eta^*$ where H is the depth, and $2\eta^*$ is the tidal range.

(b). $1n\frac{r^2}{\Delta s^2}$ versus $1n\ 2\eta^*$ where r is the distance from the centroid and Δs is the grid length. Results taken from the numerical model.

$$v_n^* = \left(\frac{g}{H}\right)^{1/2} \eta_n^* \tag{17}$$

$$c = \frac{r\sigma}{n} = (gH)^{1/2}$$

where c is the phase velocity, and a is a constant.

This circular mode is essentially a Kelvin Wave. If σ_0 and f have opposite signs, i.e. for a clockwise tide in the northern hemisphere, and a counterclockwise tide in the southern hemisphere the amplitude of the wave decays with r.

The total energy (E_n) of the parabolic shelf Kelvin Wave has a simple representation,

$$E_n = 2\pi\varrho g a_2^2(1 + f/\sigma_0)\left(1 - \left(\frac{a_1}{a_2}\right)^{2(1+f/\sigma_0)}\right) A_n A_n^*$$

and thus, the fraction of energy lost per cycle,

$$\varphi_n = 2B_n B_n^* \Big/ \left(\varepsilon^2\left(n^2 - \frac{f^2}{\sigma_0^2}\right)\left(1 + \frac{f}{\sigma_0}\right)\left(1 - \frac{a_1}{a_2}\right)^{2(1+f/\sigma_0)}\right) A_n A_n^*\Big). \tag{18}$$

b. Application to the New Zealand semi-diurnal tide. For the New Zealand semi-diurnal tide $f = -10^{-4}\ s^{-1}$ and $\sigma = 1.4\times10^{-4}\ s^{-1}$ hence $f/\sigma = -0.7$. The spatial variation of the tide in the numerical solution is shown in Fig. 7. The best fit power laws for the tidal amplitude (η^*) against the depth H, and against the distance from the centroid of the model r are

$$\eta^* = 2.25\left(\frac{r}{\Delta s}\right)^{-0,68\pm,02} \tag{19}$$

and

$$\eta^* = 6.85\, H^{-0,34\pm,01} \tag{20}$$

where $\Delta s = 111$ km, which may be combined to yield,

$$H = 0.21\times10^{-8} r^2. \tag{21}$$

Equation (21) is remarkably close to the equation for the parabolic shelf, with $\sigma_0 = 1.4\times10^{-4}\, s^{-1}$, and equation (19) to that for the fundamental parabolic shelf Kelvin Wave ($n = 1$, $\sigma = \sigma_0$); the exact relations for which, from equations (6) and (15) are,

$$H = 0.20\times10^{-8} r^2 \quad \text{and} \quad \eta^* = \alpha r^{-0,7}.$$

It is concluded that the semi-diurnal tide in the numerical model is very close to a parabolic shelf Kelvin Wave.

The dimensions taken to be representative of the New Zealand island shelf model are $a_1 = 280$ km and $a_2 = 1400$ km which yield a depth of 160 m at the coast, and assuming continuity of the depth at the edge of the shelf ($\varepsilon = 1$), 4000 m for the deep ocean. The co-range and co-tidal lines for the parabolic shelf wave ($n = 1$), with unit amplitude at the edge of the shelf, are shown in Fig. 8a. A forcing for the shelf wave is now introduced which allows a complete analytical solution to be evaluated.

c. Forcing by a plane wave. A progressive wave of unit amplitude, with horizontal crests, travelling in the far ocean ($r \to \infty$), along Ox is represented by the equation,

$$\zeta = e^{i(k_2 x - \sigma t)}$$

which is a solution of equation (4). Using a well known result (cf. Longuet-Higgins, 1967), the expression of ζ in circular modes yields

$$\zeta_n^*(r) = iJ_n(k_2 r)$$

where $J_n(x)$ is the Bessel function of the first kind.

The corange and cotidal lines given by equation (8) with the A_n and B_n ($n = -10 \ldots 10$) given by equations (10) and (11) for the New Zealand geometry, are shown in Fig. 8. The forced solution with $\sigma_0 = \sigma$ (Fig. 8b), indicates an amphidromic point just beyond the edge of the parabolic shelf on the left hand side of the progressive wave. (At least one amphidromic point is necessary for the phase distribution around the coast to be embedded in a progressive wave). Fig. 9 indicates that in fact, only the $n = 0$ and $n = 1$ modes are significant at the coast, and their sum gives rise to the amphidromic point.

A comparison with the World tidal charts (Hendershott, 1973), shows that indeed there is an amphidromic point associated with New Zealand and its location about

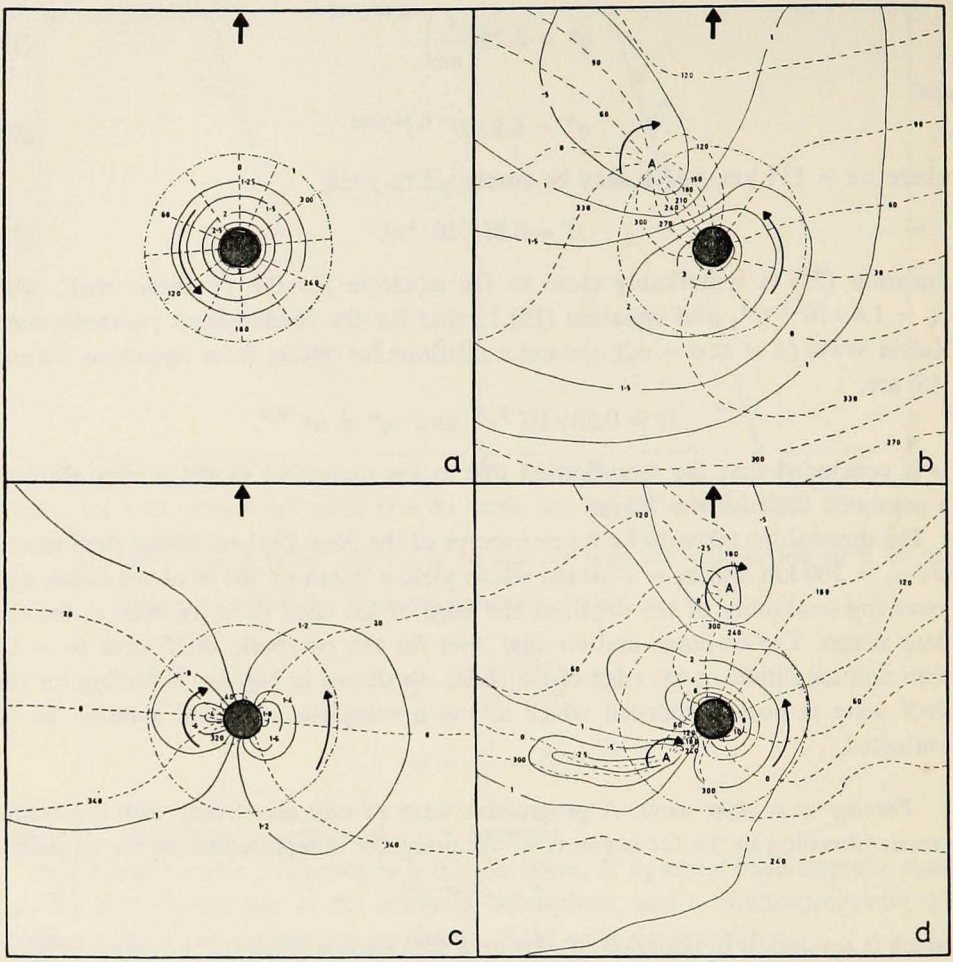

Figure 8. Contours of equal phase (φ^0) and contours of the amplification factor (A) from solutions of the island-shelf model.

(a). Parabolic shelf Kelvin wave for the shelf parameter $\sigma_0 = \sigma$.

(b). Forcing due to a wave with horizontal crests travelling in the direction of the arrow, and with the zero phase line at $r \to \infty$ passing through the origin, for the shelf parameter $\sigma_0 = \sigma$.

(c). As for (b) with $\sigma_0 = 3\sigma$.

(d). As for (b) with $\sigma_0 = {}^1/_2\sigma$.

Dashed lines are phase, solid lines are amplitude. The outer circle denotes the edge of the parabolig shelf.

2000 km to the south-south east (on most charts), is consistent with a tidal wave approaching from between the north and the north-east and thus travelling down the east coast of Australia.

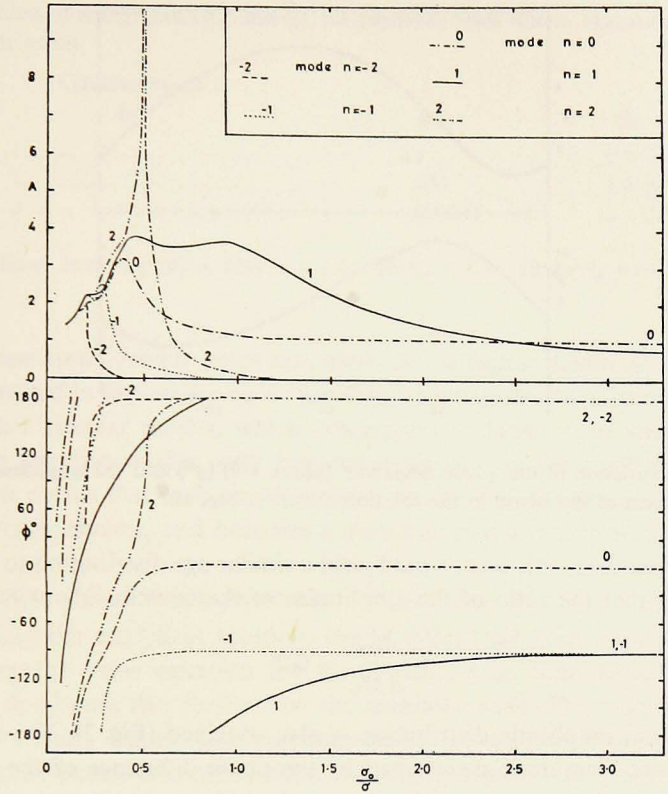

Figure 9. The phase (φ^0) and amplification factors (A) at the coast of the island for the circular modes ($n = -2, -1, 0, 1, 2$) in the solutions shown in Fig. 8.

The ratio of the amplification at the coast to the amplification at the edge of the parabolic shelf of about three is similar to observation. It may be that the relatively rapid phase change south of New Zealand reflects the presence of the amphidromic point, however, it may be due to topographic effects (cf. Section 3).

Let us examine the phase distribution of the trapped wave in more detail. It is clear that if two tidal constituents are each dominated by a *single* circular mode, the phase differences between the constituents, irrespective of frequency, will be identical at all locations on the coast. Any variation of phase difference (or age of the tide), must be due to departures from the circular symmetry produced by other modes. Fig. 10 shows the departure corresponding to Fig. 8 b, which has an amplitude of approximately 20°. Assuming that the pattern for a slightly different frequency is basically similar, it is apparent that significant differences in phase can occur if the progressive waves of each frequency *approach from different directions.*

This is suggested as the basic reason for the observed variation in the age of the tide around New Zealand. A superposition of an M_2 tide from the north-east, with

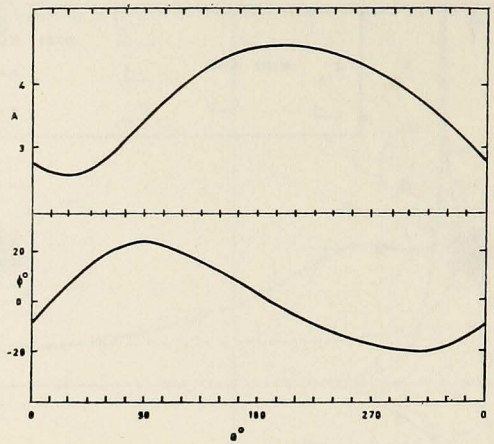

Figure 10. The variation of the 'phase deviation' (phase $-\theta$) (φ^0) and the amplification factor (A) around the coast of the island in the solution shown in Fig. 8b.

and S_2 tide from the north-west, would yield a similar age distribution to observation, and assuming that the ratio of the amplitudes of the constituents at $r \to \infty$,

$$\frac{AS_2}{AM_2} = 0.2$$

a similar coastal amplitude distribution is also obtained (Fig. 2). The origin of the phase difference diagram is determined by the phase difference of the two incident plane waves, which is not the main concern here; however, it appears that the S_2 tide is delayed by about 120° over the M_2 tide for the best agreement with observation.

The amphidromic point associated with the S_2 tide would accordingly lie further north than for the M_2 tide (compare, Bogdanov and Magarik, 1967 with Hendershott, 1973). A cause for the difference in the angle of approach of the tidal wave could be the semi-diurnal resonance which lies off north-east Australia, at a frequency intermediate between the M_2 and S_2 frequencies (Webb, 1973b). It may thus be misleading, in the case of New Zealand, to associate the changes in age with local resonant effects. The phase and amplitude changes in Fig. 9 are consistent with the weak maximum in the observed admittance at about the frequency of the M_2 tide (Fig. 3).

The effect of varying the dimension of the shelf-island system on which the tidal wave impinges, over a wider range, may be of interest. The resultant tide is governed by the ratio of the shelf radius to the wavelength, since,

$$a_2 k_2 = 10^{-4} \sigma_0^{-1}.$$

For a small shelf no amphidromic point exists and the amplification factor tends to unity as $\sigma_0 \to \infty$. As the shelf is widened a virtual amphidromic point (Fig. 8c) emerges to give tides similar to the New Zealand situation for $\sigma_0 \sim \sigma$. For a wider shelf,

Table 3. Fraction of energy lost (φ_n) and Q_n for parabolic shelf Kelvin Waves forced by a plane wave in the far ocean.

Circular Mode (n)	φ_n	Q_n
1	4.7	1.3
2	.044	$1.4\ 10^2$
3	.000047	$1.3\ 10^5$

Results calculated from Equation (18) $\sigma = 1.4 \times 10^{-4}\, s^{-1}, f = -10^{-4}\, s^{-1}$, $\varepsilon = 1$, $\frac{a_1}{a_2} = 0.2$, and $\sigma_0 = \sigma_n$.

more than one amphidromic point may exist, as the higher modes in turn dominate. This is illustrated in Fig. 8d for $\sigma_0 = {}^1/_2\sigma$. The trapping efficiency increases markedly for the higher circular modes, which correspond to larger shelf widths, (Table 3, Fig. 9). The negative modes only become important as the shelf width increases (Fig. 9). This means that each circular mode pair (n, $-n$) is essentially a progressive wave on narrow shelves, and becomes a standing oscillation on wider shelves.

d. The variation of the Coriolis parameter ('β effect')

In obtaining the analytical solution, the 'β effect' has been omitted. It is easily shown, using the wave equation for the β-plane, (e.g. Summerfield, 1969), that bathymetry dominates the 'β effect' on the parabolic shelf. The main interest of the analysis lies in this region, and the immediately contiguous deep ocean. The far deep ocean (an f-plane, of constant depth) should be regarded only as a very idealized model, necessary to complete the solution. In view of the simplifications of the analytical model, including of course the presentation of the New Zealand sub-continent as a circular massif, the overall agreement between theory and data appears adequate.

5. Conclusons

The model of the New Zealand semi-diurnal tide indicates that New Zealand has a highly significant effect on the propagation of the tidal wave, not only on its own continental shelf, but through the associated amphidromic point, also on the deep sea tide. The exact position of the amphidromic point for each semi-diurnal tidal constituent is a response to the total New Zealand bathymetry, and also the direction of the propagation of the deep sea tidal wave. The significance of this result, and possibly analogous results in other parts of the ocean, should not be overlooked in numerical modelling.

It would be very interesting to carry out a set of deep sea tidal measurements to examine the distribution of amphidromic points for the semi-diurnal species off the south and east coasts of New Zealand, which have been shown to be one of the main features of the tidal regime.

Acknowledgements. Helpful comments by a referee and by Dr. D. E. Cartwright are gratefully acknowledged.

REFERENCES

Bogdanov, K. T. and V. A. Magarik. 1967. Numerical solution of the distribution problem for the semi-diurnal tidal waves (M_2 and S_2) in the world ocean. Doklady Akad. Nauk SSSR *172*: 1315–1317.

Bye, J. A. T. 1975. The FLOW series of thallasso-models. Lecture Notes. The School of Earth Sciences. Flinders University of South Australia.

Carter, L. and R. A. Heath. In press. The role of the mean circulation, tides, and waves in the transport of sediment on the New Zealand contiental shelf. N. Z. Jour. of Mar. and Freshw. Res.

Doodson, A. T. and H. D. Warburg. 1941. Admiralty manual of tides. The Hydrographic Department, 270 pp.

Garrett, C. J. R. and W. H. Munk. 1971. The age of the tide and "Q" of the oceans. Deep Sea Res. *18*: 493–504.

Heath, R. A. 1973. Direct measurements of coastal currents around the southern half of New Zealand. N. Z. Jour. of Mar. and Freshw. Res. *7*: 331–368.

Heath, R. A. In press. The lunar semi-diurnal tide in Cook Strait, New Zealand. Deutsch Hydrog. Zeit.

Hendershott, M. C. 1973. Ocean Tides. EOS Transactions. Amer. Geo..Uni. *54*: 76–86.

Hydrographic Department. 1958. The New Zealand Pilot, 12th Edition. London, 500 pp.

Hydrographic Department. 1963. The Admiralty Tide Tables, Vol. III, 1964. Pacific Ocean and adjacent seas. London.

Lamb, H. 1953. Hydrodynamics. 6th ed. Cambridge University Press. 738 pp.

Lawrence, P. 1967. New Zealand region bethymetry 1:6,000,000. N. Z. Oceanographic Institute Chart, Miscellaneous Series 15.

Longuet-Higgins, M. S. 1967. On the trapping of wave energy round islands. J. Fluid Mech. *29*: 781–821.

Longuet-Higgins, M. S. 1969. On the trapping of long-period waves round islands. J. Fluid Mech. *37*: 773–784.

Matthews, J. B. and J. C. Mungall. 1972. A numerical tidal model and its application to Cook Inlet, Alaska. J. Mar. Res. *30*: 27–38.

Pekeris, C. L. and Y. Accad. 1969. Solution of Laplace's tidal equation for the M_2 tide in the world oceans. Phil. Trans. Roy. Soc. *265*: 413–436.

Summerfield, W. C. 1969. On the trapping of wave energy by bottom topography. Horace Lamb Centre Res. Pap. *30*. Flinders University of South Australia.

Summerfield, W. C. 1972. Circular islands as resonators of long-wave energy. Phil. Trans. Roy. Soc. A *272*: 361–402.

Webb, D. J. 1973a. On the age of the semi-diurnal tide. Deep Sea Res. *20*: 847–852.

Webb, D. J. 1973b. Tidal Resonance in the Coral Sea. Nature *243*: 511.

Received: *12 June, 1974*; revised: *28 April, 1975.*